Kinetochore Structure: Electron Spectroscopic Imaging of the Kinetochore

J. B. Rattner and D. P. Bazett-Jones

Departments of Medical Biochemistry and Anatomy, Faculty of Medicine, The University of Calgary, Calgary, Alberta T2N 4N1, Canada

Abstract. The structure of the kinetochore in thin section has been studied in the Indian muntjac by an electron spectroscopic imaging technique. This procedure allows the analysis of the distribution of phosphorus within the layers of the kinetochore. The results indicate that this element is a major component of both the inner and outer plates whereas it is largely absent in the middle plate and fibrous corona. The majority of the phosphorus is localized to a 30-nm fiber(s) that is woven through the layers of the kinetochore. The presence of phosphorus within this fiber, along with its morphological and biochemical features, indicates that it contains DNA. The fiber(s) occupies a major portion of the inner and outer plate where it forms a series of rows. It is rarely observed in the middle layer except where it passes between the inner and outer layers. The absence of structure in the middle plate suggests that it may represent a space rather than a plate that in turn may be related to the function of this region. The distribution of phosphorus within the kinetochore is neither altered by treatment with colcemid nor by the presence of microtubules at the kinetochore. Analysis of conventional micrographs of the kinetochore together with structural information obtained by electron spectroscopic imaging suggests that most microtubules insert and terminate between the rows of kinetochore fibers in the outer plate. However, some microtubules continue through the middle layer and terminate at the lower plate. The insertion of microtubules at different levels of the kinetochore may reflect the existence of functionally distinct microtubule classes. Electron spectroscopic imaging indicates that the microtubules associated with the kinetochore are phosphorylated.

DESPITE the complex nature of the metaphase chromosome, there is little structural indication of regional differentiation except within the primary and secondary constrictions. The primary constriction is unique in that it contains the most structurally complex region of the chromosome, the kinetochore. In early electron microscope studies, the kinetochore was described as a roughly circular structure composed of three plates stacked on top of one another at the outer surface of the primary constriction (1, 2). Further analysis of thin sections and whole mount preparations of the kinetochore have indicated that fibers are present within the kinetochore region and that these fibers interact directly with spindle microtubules (3). It has been possible to examine the relationship between the plates and the fibers through the study of intact kinetochores that have been released from the chromosome after nuclease digestion (4). Whole mount electron micrographs of these isolated kinetochores illustrate that the outer plate is formed in part by the parallel stacking of lengths of a 30-nm fiber(s) across the plate. This arrangement can also be visualized in kinetochores of intact chromosomes by scanning electron microscopy (5).

Several lines of evidence have suggested that the kinetochore fiber contains DNA. Ultrastructural studies indicate that the organization of the fiber is similar to that of the 30-nm fiber found in bulk chromatin (4). That is, the higher order 30-nm kinetochore fiber is formed by the folding of a fiber with a diameter of 10 nm. The beaded appearance of this smaller fiber class is compatible with the observation that a subset of nucleosomes can be identified that are associated with kinetochore-specific proteins (6). Kinetochore fibers are also susceptible to nuclease attack although they are more resistant than bulk chromatin. This feature has been exploited in studies designed to identify kinetochore-specific sequences (7). Differential susceptibility to nucleases may indicate that the protein composition and packing arrangement of the kinetochore fiber differs from that of chromatin found in the remainder of the chromosome. This may account for the difference between the electron density of the kinetochore region and the remainder of the chromosome noted in many studies (4, 8). The DNA, and its associated proteins, could play a dual role in the kinetochore, determining its gross structure and specifying the interaction of the kinetochore with spindle microtubules.

While the studies described above have provided some detail concerning the organization of the kinetochore outer plate, there is still little information defining the arrangement of the kinetochore fiber within the lower two plates or the

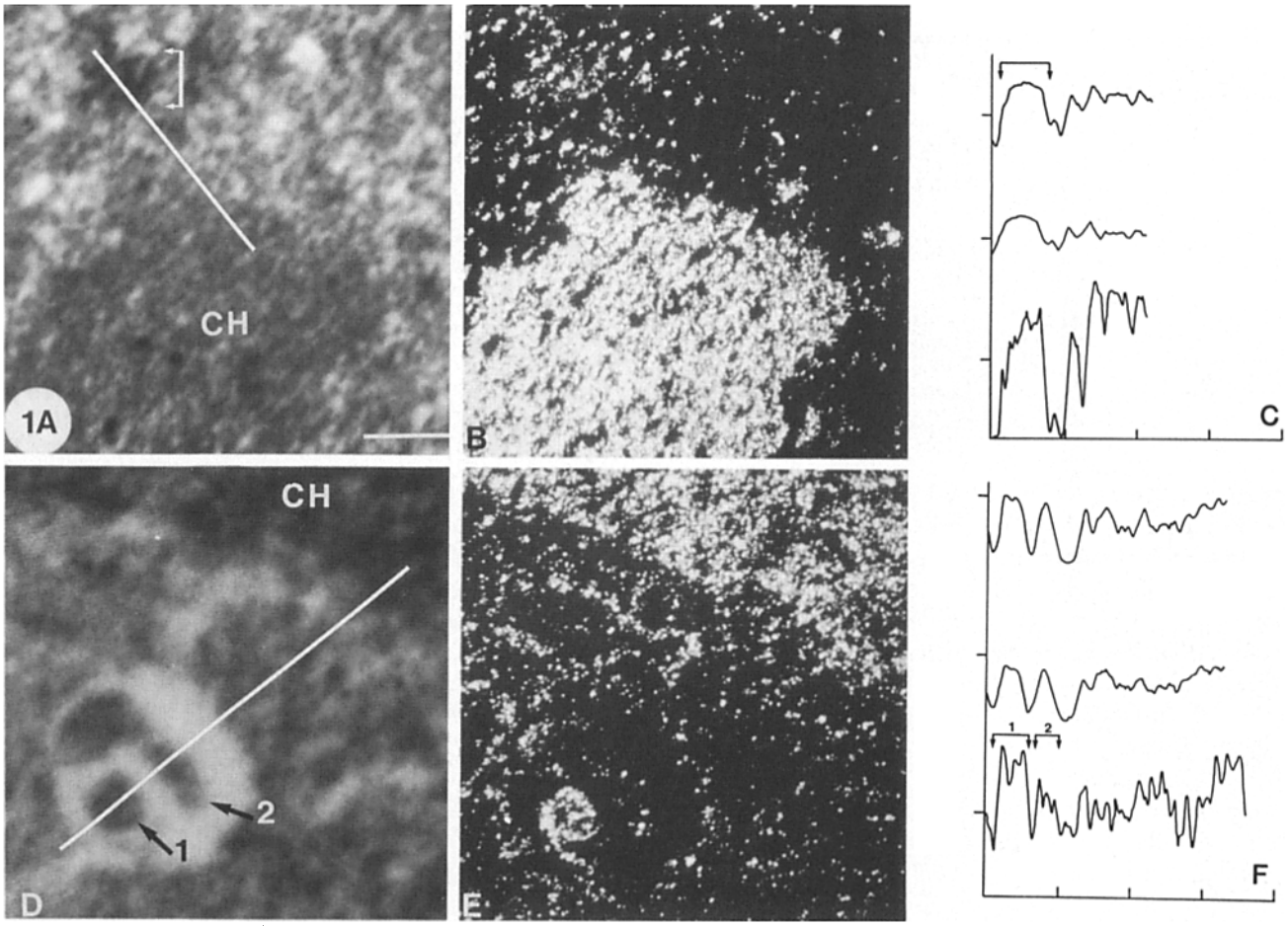

Figure 1. Micrographs illustrating the reference images (*A* and *D*), recorded at 120 eV energy loss, of regions near the edge of a chromosome (*CH*), obtained from a mitotic Indian muntjac cell. Net phosphorus images of the identical regions are shown in *B* and *E*, phosphorus being represented by white areas in the image. The five-pixel-wide line scans of the optical density of the indicated regions in the phosphorus-enhanced, reference, and net phosphorus images (*top to bottom*) are shown in *C* and *F*. The gain of the signal was increased to generate the line scans in the net images. Bar, 0.3 μm.

precise relationship of the fiber in the outer plate to elements of the spindle. Further, the composition and precise relationship of the fibrous corona, which lies along the surface of the kinetochore, to the fibers of the outer plate remains unknown.

To address these questions, we have combined conventional electron microscopy with a new analytical technique called electron spectroscopic imaging (ESI).[1] Within the electron microscope incident electrons pass through the specimen and cause excitations and ionizations of the specimen's atoms. It is possible to analyze this information in terms of x-ray emission spectra or with the energy spectra of electrons that have passed through the sample. The energy loss spectrum reflects the sample's chemical composition. Recently an electron microscope has been developed in which a parallel electron spectrometer had been installed within the microscope so that spectra can be obtained and images can be recorded at any particular energy loss. This microscope can produce a two-dimensional distribution map of a particular chemical element characterized by both high spatial resolution and sensitivity. This technique has been applied to the detection of phosphorous within the basic 10-nm chromatin fibers and the resolution of this technique is sufficient to allow the detection of the path of the DNA around individual nucleosomes (9, 10). If the kinetochore fiber contains DNA, then the path and distribution of this fiber within the kinetochore can be determined in thin sections by the electron spectroscopic analysis of the phosphorus distribution within the kinetochore plates. In this report, we describe the application of ESI to the study of the organization of the kinetochore of the Indian muntjac. We describe the precise distribution of phosphorus and the 30-nm kinetochore fiber within each of the regions of the kinetochore. Our findings provide a basis for the correlation of the structure of the kinetochore with its role in capturing and regulating microtubule length.

Materials and Methods

Cell Culture and Conventional Electron Microscopy

Fibroblast cells of the Indian muntjac (Muntjac muntjac), an asiatic deer, were grown in monolayer culture in RPMI media supplemented with 10% FCS. Mitotic cells were obtained by selective mitotic detachment from

1. *Abbreviation used in this paper*: ESI, electron spectroscopic imaging.

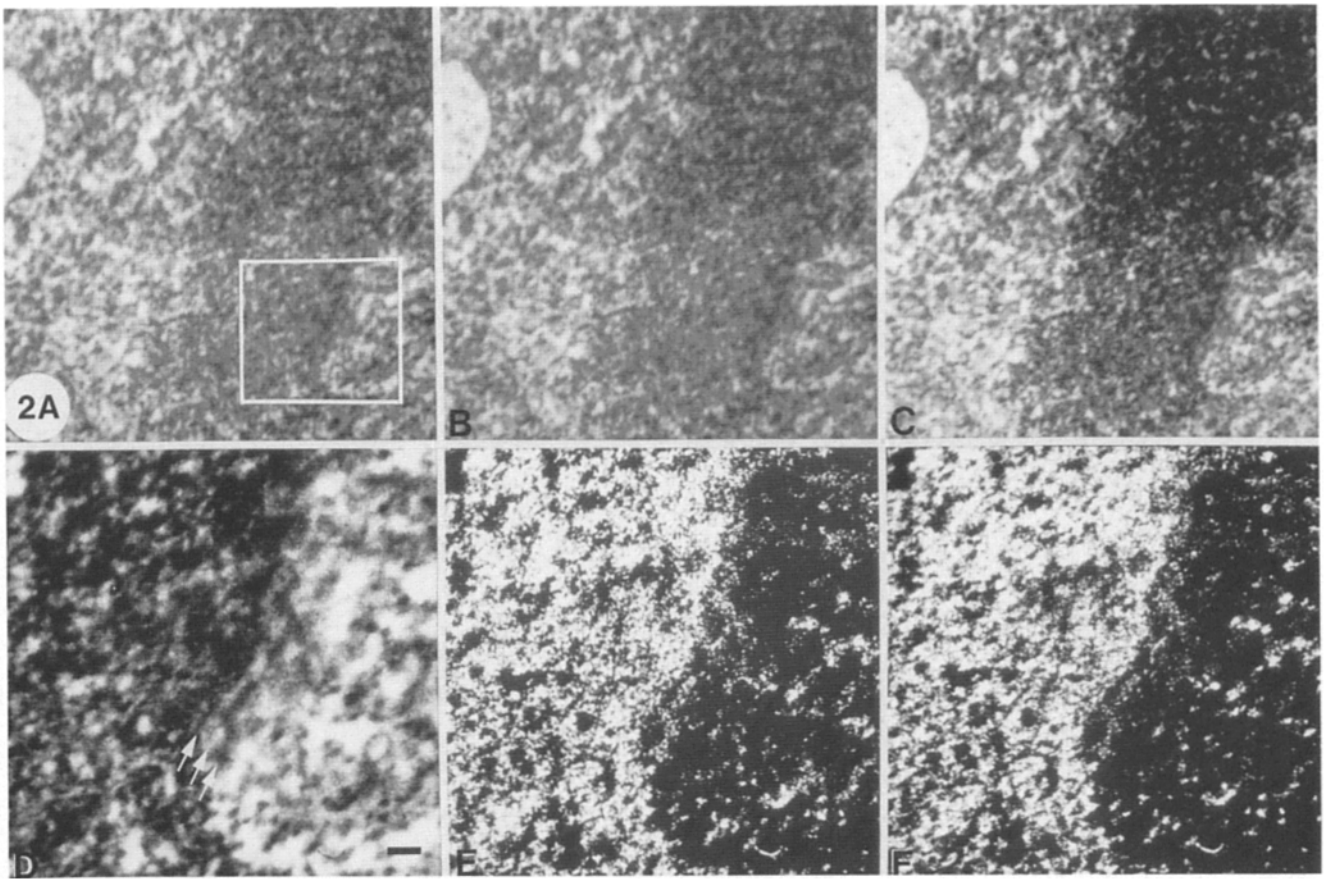

Figure 2. Micrographs illustrating reference images recorded at 100 and 120 eV (*A* and *B*) and a phosphorus-enhanced image recorded at 180 eV (*C*) of a region containing a chromosome from a mitotic Indian muntjac cell. The box includes a kinetochore, used to compare the one-parameter and two-parameter spectral background extrapolation methods. A net phosphorus image using a two-parameter and a one-parameter background extrapolation is shown in *E* and *F*, respectively. Bar, 90 nm.

logarithmically growing cultures and pelleted and fixed for 1 h in 3% glutaraldehyde in a phosphate-free buffer (1 mM sodium barbitol buffer, pH 7.4). The cell pellet was then washed in buffer and postfixed for 1 h in a 1% OsO_4 solution buffered in a similar manner. The specimens were then washed in water and passed through a graded ethanol series and embedded in Spurs resin. Sections 30 nm in thickness were cut from blocks and placed on copper grids. For standard transmission microscopy, the cells were prepared as described above, substituting Millonig's phosphate buffer for the Barbitol buffer, and sections in the silver to gold range were collected. The specimens were examined in a Hitachi H-500 electron miroscope operated at 50 kv.

Electron Spectroscopic Imaging

ESI was performed on a Zeiss EM 902 electron microscope equipped with a prism-mirror-prism type electron imaging spectrometer. The microscope was operated at an acclerating voltage of 80 kV. However, it is designed so that the focus is maintained at all energy losses because the accelerating voltage is increased by the amount of energy loss that has been selected. This has the additional benefit that the energy selecting slit aperture does not have to be repositioned when a different region of the energy loss spectrum is selected. The width of the slit aperture corresponded to 12 eV. A 600-μm condenser and a 40-μm objective aperture were used.

The specimen grids were scanned to find regions of interest using low energy loss electrons, in the range of 20–30 eV, to minimize the radiation exposure to the specimen. The contrast of the unstained sections was greater in this part of the spectrum than if only elastically scattered electrons were used to form a bright field image. Specimen irradiation was minimized even further by focussing on a nearby region before the beam was shifted away and the relevant area positioned for photographing. If multiple exposures of a region were to be recorded at different energy losses, the beam was shifted away while the new region of the energy loss spectrum was selected. Electron micrographs were recorded at a magnification of 14,000 and to an optical density not exceeding 0.4. Images were recorded on sheet film with the electron image emulsion SO-163 (Eastman Kodak Co., Rochester, NY) which was subsequently processed in full strength D-19 developer (Eastman Kodak Co.) for 12 min. To produce an image at an energy loss of 120 and 180 eV, an electron exposure of 0.7×10^4 electrons/nm^2 and 1.6×10^4 electrons/nm^2, respectively, was required. These values were obtained from current measurements with a Faraday cage detector.

A phosphorus distribution map cannot be generated simply by recording an image in a region of the spectrum corresponding to a phosphorus ionization edge. The reason for this is that the ionization edges of the inner shell electrons of the lighter elements are generally superimposed on a rapidly declining plasmon-like background whose contribution must be eliminated to produce the net elemental image. To do this, it was necessary to record a reference image at an energy loss before the ionization edge and an element enhanced image on the peak of an ionization edge of the element. For the phosphorus $L_{II,III}$ ionization edge, reference images were recorded between 110 and 120 eV energy loss and the phosphorus enhanced image between 150 and 180 eV. Relevant areas of the micrographs were digitized using a linear, high resolution video camera (Bosch, West Germany) connected to a computer equipped with image analysis software. Normalization factors were calculated over regions in the reference and phosphorus-enhanced images that were known to be devoid of phosphorus such as the plastic embedding matrix. These factors were used to compensate for slight differences in photographic intensities between the images.

A net phosphorus image was then generated using two approaches. The first involved aligning the reference image with respect to the phosphorus-enhanced image to within a pixel before subtracting the first from the second image. The production of a net elemental image using this approach could be inappropriate because mass-density effects can introduce nonlinearities

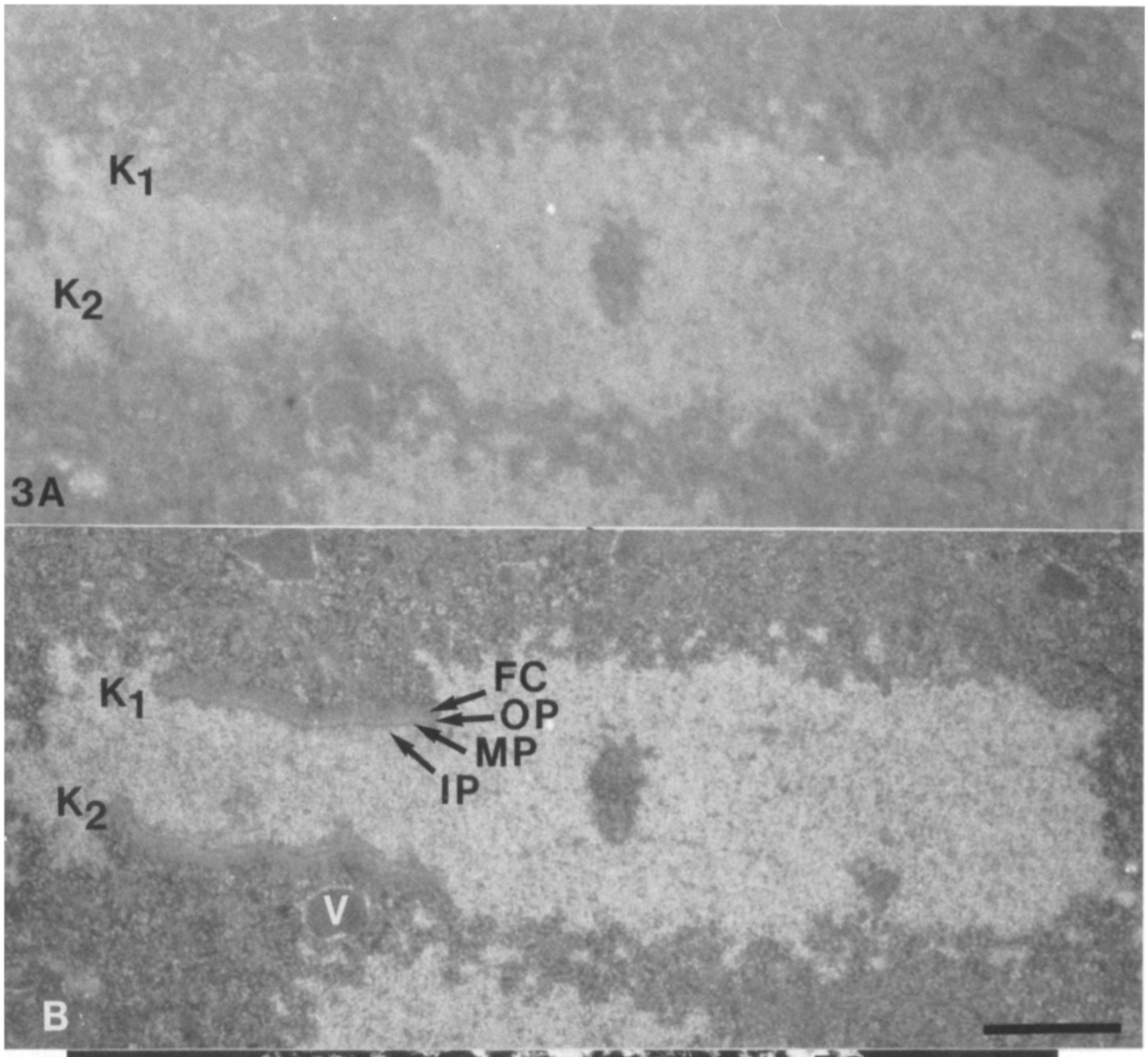
K1
K2
3A
K1
FC
OP
MP
IP
K2
V
B

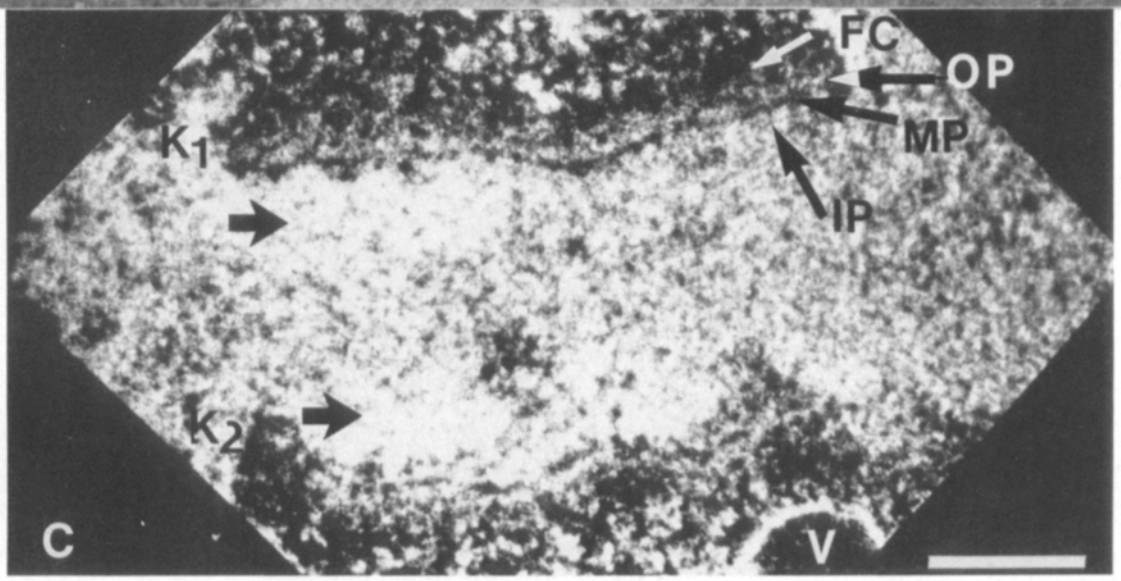
FC
OP
MP
IP
K1
K2
C
V

from multiple scatter and local changes in the energy loss spectrum that thereby produce a false signal. To avoid this potential problem, two or more reference images were used to extrapolate a correct value at any pixel, thereby producing a corrected reference image to which the phosphorus-enhanced image could be compared. The extrapolation of the energy loss spectrum under the ionization edge was based on the relationship

$$I = AE^{-R}, \qquad \text{(eq. 1)}$$

where I represents the intensity in the energy loss spectrum, E is the energy loss, and A and R are constants whose values must be calculated for any point in the image (11). A one-parameter fit makes use of only one reference image, whereas this two-parameter fit requires at least two reference images to calculate the two unknowns, A and R. However, a one-parameter fit was generally employed since a comparison of the two approaches gave similar results.

Elemental Imaging of Phosphorus

The ability of ESI to detect and to map particular elements in biological specimens with high sensitivity and resolution has been the subject of several studies. Investigations of the phosphorus distributions in nucleoprotein complexes (9, 10) have demonstrated the limits of detection and the potential in resolving meaningful structural information with this technique. Whereas the technique is potentially powerful, the sources of error and artifact must be realized before confidence in such maps can be justified. A major source of error arises from the removal of the contribution to an elemental map arising from a high background in the energy loss spectrum on which the discrete elemental ionization edges are superimposed. An inaccurate extrapolation would lead to false signal being generated in regions that have higher mass-density. To be confident that the phosphorus distribution maps of the kinetochore regions are reliable we have compared the results where two extrapolation algorithms have been used to determine the extent of the mass-density contribution to false signal.

One-Parameter Spectral Background Correction

Because the phosphorus spectral ionization edge is superimposed on a broad exponentially decaying background in the energy loss spectrum, it is necessary to record images from at least two regions of the energy loss spectrum, one at an energy loss on or just above the phosphorus $L_{II,III}$ ionization edge (phosphorus-enhanced image) and at least one image at an energy loss less than that of the ionization energy (reference image). The distribution of phosphorus at high resolution is subsequently generated by the subtraction of the reference from the phosphorus-enhanced image. The strict requirement of this approach is that the specimen be thin, as thin as 30 nm for an accelerating voltage of 80 kV, to ensure that multiple scattering events be infrequent. Otherwise, a false positive phosphorus signal could result in the net images over regions that have greater mass-density.

In this article we claim that certain components of the kinetochore contain significant levels of phosphorus. Because some of these regions, however, are also regions that are high in mass-density, a portion of the associated phosphorus signal may be an artifact. To test this, we examined the micrographs to determine whether structures other than kinetochores existed that had mass-density equivalent to that of kinetochores but did not generate a high phosphorus signal. Many such structures indeed exist in the micrographs, two of which are illustrated in Fig. 1. Reference images from regions of micrographs that also contain kinetochores are shown (*A* and *D*). The edge of a chromosome is indicated by *CH* in *A* and is also seen across the top of *D*. Fig. 1, *B* and *E*, represent the net phosphorus images of these two regions obtained by the one-parameter extrapolation method. Optical density profiles of the features intersected by line scans obtained from an average of five pixels in width over the indicated regions were generated for each of the phosphorus-enhanced images, the reference images, and the net phosphorus images (top to bottom), represented in Fig. 1, *C* and *F*. The reference and phosphorus-enhanced images were normalized by equating optical densities over regions of plastic, phosphorus-free regions. In Fig. 1 *A*, the structure indicated by the bracket can be seen to have a marginally greater mass density than the adjacent phosphorus-rich chromosome. However, the phosphorus content of this structure is less than the average representation of phosphorus in the chromosome, demonstrated in the net phosphorus image (Fig. 1 *B*) and also by the use of the line scans. This demonstrates that an object of mass density equal to that of the chromosome does not generate a detectable false phosphorus signal by mass-density effects. A similar demonstration is made in *D–F*. The objects labeled *1* and *2* (in Fig. 1 *D*) have approximately the same mass-density as seen in the reference image and further demonstrated by the line scan of the reference image. The net phosphorus distribution, however, demonstrates that only the structure labeled *1* has a phosphorus content significantly greater than the surrounding area. This demonstrates that objects of comparable mass-density can produce phosphorus distributions showing very different levels. This has already been demonstrated in macromolecular studies using ESI (10). These net phosphorus images were produced with a one-parameter extrapolation algorithm. Although these images clearly demonstrate that mass-density effects do not cause detectable artifacts in the specimens used in this study, we did compare our results using the one-parameter extrapolation method with a more stringent two-parameter spectral background correction algorithm.

Two-Parameter Spectral Background Correction

The intensity of the spectral background on which the phosphorus elemental ionization is superimposed decays logarithmically (see eq. 1 in Materials and Methods). The recording of two or more reference images allows the calculation of the parameters A and R for every point in the

Figure 3. The reference (*A*), phosphorus-enhanced (*B*), and net phosphorus (*C*) images of the X+3 chromosome of the Indian muntjac from a cell arrested with colcemid. The chromosome is sectioned so that both sister kinetochores (*K1* and *K2*) are seen in cross section. Four regions of the kinetochore can be identified: the fibrous corona (*FC*), the outer plate (*OP*), the middle plate (*MP*), and the inner plate (*IP*). In the net phosphorus image (*C*) regions rich in phosphorus appear white. These include the inner and outer kinetochore plates and the membranes of cytoplasmic vesicles (*V*). The whole chromosome is rich in phosphorus and a particularly strong signal is apparent along the margins of the centromere (*large arrows*). Bars: (*A* and *B*) 1.6 μm; (*C*) 0.3 μm.

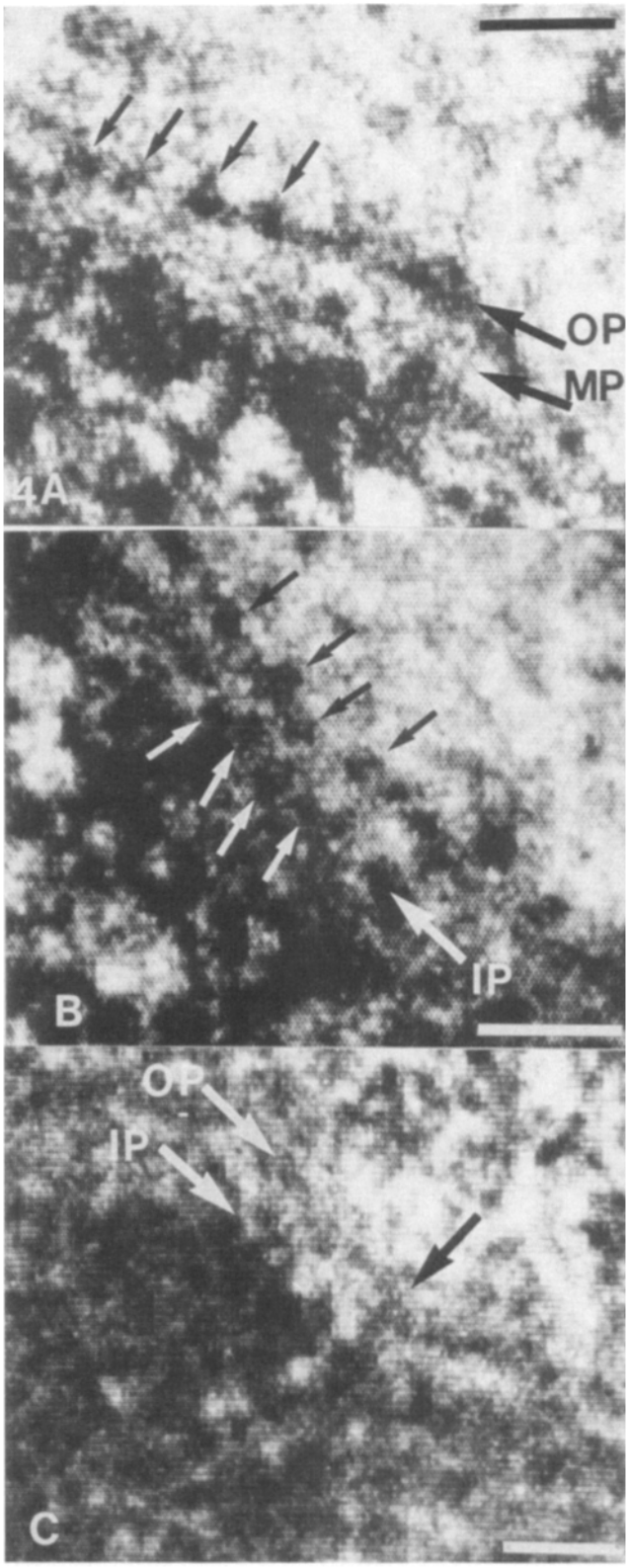

Figure 4. High magnification net phosphorus images of cross sections through the kinetochore region of an Indian muntjac chromosome from a cell arrested with colcemid. In these micrographs, phosphorus-rich regions appear black. In the outer plate (*OP*) the major phosphorus signal is found in 30-nm profiles (*arrows*) arranged in a tandem array along the plate. The middle plate (*MP*) is devoid of a strong phosphorus signal. The inner plate (*IP*) also contains phosphorus rich 30-nm profiles (*B, white arrows*) similar to those found in the outer plate (*black arrows*). Occasionally, it is possible to detect a phosphorus-rich fiber (*C, black arrow*) extending between the inner (*IP*) and outer (*OP*) plates of the kinetochore. Bar, 0.16 μm.

image and thereby permits the generation of a corrected reference image, one that would better compensate for mass–density effects. We compared the net phosphorus images generated from both a one-parameter and two-parameter background extrapolation on a region containing a kinetochore structure.

Micrographs used for this analysis are represented in Fig. 2. Reference images recorded at 100 and 120 eV, before the phosphorus ionization edge, are shown in *A* and *B*, respectively. A phosphorus-enhanced image, recorded at 180 eV is represented in Fig. 2 *C* and an enlarged view of the indicated area of the 180 eV image is represented in *D*. Qualitatively, the two reference images are identical, whereas the contrast of the chromosomes are enhanced significantly in the 180 eV image. Also, the 180 eV image is slightly sharper, having greater resolution. The explanation for this is that the lower energy loss images are created by electrons that have lost energy due to spatially delocalized events (plasmon-like excitations). In contrast, a greater fraction of the energy loss events that are represented in the 180 eV image result from discrete, localized events, particularly those involved in ionizing individual phosphorus atoms. Appropriate normalization of the three images was carried out over regions of plastic, devoid of phosphorus to correct for slight variations in photographic density. A net phosphorus image of the enlarged region using a two-parameter and a one-parameter background extrapolation are shown in Fig. 2, *E* and *F*, respectively. The kinetochore plates are indicated by arrows in the phosphorus enhanced image in Fig. 2 *D*, the inner, middle, and outer plates, from left to right. The net phosphorus images of the kinetochore using either extrapolation are nearly indistinguishable. The outer plate of the kinetochore in both can be seen to contain phosphorus. This result provides confidence in the analysis where a one-parameter extrapolation was used, data that had been collected before developing computer software to calculate multiple-parameter extrapolations.

Kinetochore Structure of the Muntjac

The karyotype of the Indian muntjac is unique among the mammals having the smallest number of chromosomes (2n = 6 ♀ 7 ♂). These chromosomes are extremely large and contain extensive centromere regions. It has been suggested that the karyotype of the Indian muntjac has evolved through a series of Robertsonian fusions from an ancestral species, the Chinese muntjac (2n = 46). In thin section, the kinetochores of the Indian muntjac display a typical tri-lamellar morphology. However, several lines of evidence suggest that they are compound in nature, composed of several unit kinetochores that are visible at interphase. At cell division, these unit kinetochores fuse to form a single functional kinetochore (12, 4). The unusually large size of the muntjac kinetochores makes them ideal for ultrastructural studies.

Elemental Imaging of Phosphorus in the Kinetochore

To determine the distribution of phosphorus within thin sec-

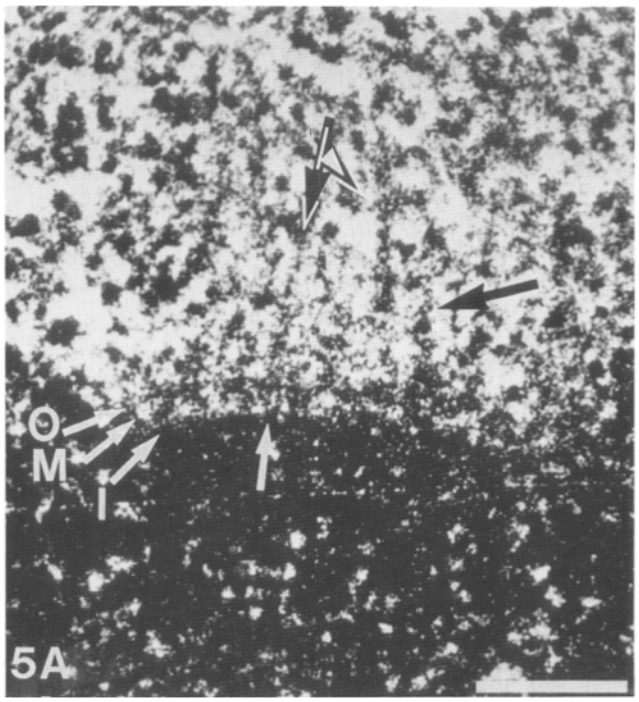

Figure 5. The net phosphorus image of a kinetochore that is associated with spindle microtubules. A phosphorus signal is still associated with the outer (*O*) and inner (*I*) plates and absent from the middle (*M*) plate. Microtubules also appear phosphorylated (*arrows*). Most terminate in the outer plate but some insert directly into the lower plate (*white arrow*). Bar, 0.3 μm.

tions containing the kinetochore of the Indian muntjac, two micrographs were taken of each area of interest, a reference image and a phosphorus-enhanced image. The reference image was then computer subtracted from the phosphorus image to produce a net phosphorus image (see Materials and Methods) which is an elemental distribution map of the area of interest. It should be noted that all the sections are viewed unstained and the section thickness did not exceed 30 nm, the thickness of a single kinetochore plate. The disadvantage of requiring extremely thin sections, a requirement of successful elemental mapping, is compensated by better resolution and a facilitated interpretation of the observed structures.

Fig. 3 *A* is a micrograph illustrating the reference image of the X+3 chromosome of the Indian muntjac from a cell arrested with colcemid. This chromosome contains the largest centromere and kinetochore region of the karyotype. The phosphorus-enhanced image for this chromosome is presented in Fig. 3 *B*. It is clear in these unstained micrographs that this chromosome has been cut so that sister kinetochores (*K1* and *K2*) are viewed in cross section. Four regions can be easily identified, the inner plate, the middle plate, the outer plate, and the fibrous corona. The kinetochore sits in a cup like depression in the chromosome. Chromatin adjacent to the kinetochore can be seen extending out over the lateral margins of the kinetochore. The surface of the chromosome in general does not have a smooth morphology, rather chromatin fibers appear to extend out from the surface of the chromosome and can be viewed in both longitudinal and cross-sectional profile. Regions that appear to lack chromatin within the body of the chromosome are characteristic for many of the larger muntjac chromosomes. These spaces may reflect the coiled nature of the metaphase chromosome (13), corresponding to less densely packed regions in the center of the coil or regions between adjacent coils.

The net phosphorus image of the kinetochore regions of the X+3 chromosome is illustrated in Fig. 3 *C*. In this image, the regions rich in phosphorus appear white whereas the regions poor in this element are black. It is clear that within the four regions denoted in Fig. 3 *B*, a strong phosphorus signal is confined to the inner and outer plates and is absent from the middle plate and the fibrous corona. As expected, the chromatin composing the body of the chromosome displays a strong phosphorus signal. Interestingly, however, the phosphorus content is greater along the margins of the centromere than in the central portion of this region, probably reflecting a differential distribution of chromatin fibers (Fig. 3 *C*, *large back arrows*). This type of distribution is compatible with the observation that the primary constriction is formed by the coiling of a higher order fiber composed of radial loops (14). Phosphorus is also detected in the cytoplasm, arising largely from ribosomes and membranes of vesicles and mitochondria.

The precise distribution of the phosphorus signal within each layer of the kinetochore can be best visualized in high magnification micrographs. It is possible to reverse the contrast of the net image within the computer to facilitate visualization. The net phosphorus images illustrated in Fig. 4, *A*, *B*, and *C*, have been treated in this way so that regions rich in phosphorus now appear black. Views of the outer plate indicate that the signal is predominantly distributed in cylindrical structures that have a diameter of 30 nm (Fig. 4 *A*). These structures are comparable to cross-sectional profiles of the 30-nm kinetochore fiber that are detected by conventional microscopy (4). It is important to note that whole mount preparations have illustrated that the kinetochore fiber follows an irregular path across the kinetochore plate (4, 5). Therefore, in cross sections of the kinetochore plate, perfect cross sections of the fiber are only occasionally detected. The phosphorus-rich profiles of the kinetochore fiber have a center-to-center spacing of ~60–70 nm. There is a lower level of phosphorus between the fiber profiles that probably originates from a protein matrix that surrounds the kinetochore fibers.

High magnification views of the net phosphorus images of the inner plate also indicate that the phosphorus signal is largely confined to 30-nm circular profiles (Fig. 4 *B*). In favorable regions, it is apparent that these profiles are distributed in a tandem array along the inner plate. This highly ordered arrangement indicates that the gross fiber organization of the inner and outer plates are similar. Once again phosphorus-containing material is also present between the fiber profiles, suggesting the presence of a phosphoprotein matrix in the lower layer of the kinetochore. It is also possible to detect random profiles of the 30-nm chromatin fiber which make up the body of the chromosome in the region underlying the inner kinetochore plate. However, the profiles do not display the highly ordered packing pattern that is visible in the kinetochore region.

In cross-sections, the middle layer of the kinetochore represents a region that is low in phosphorus. However, it is occasionally possible to detect a phosphorus-rich band that

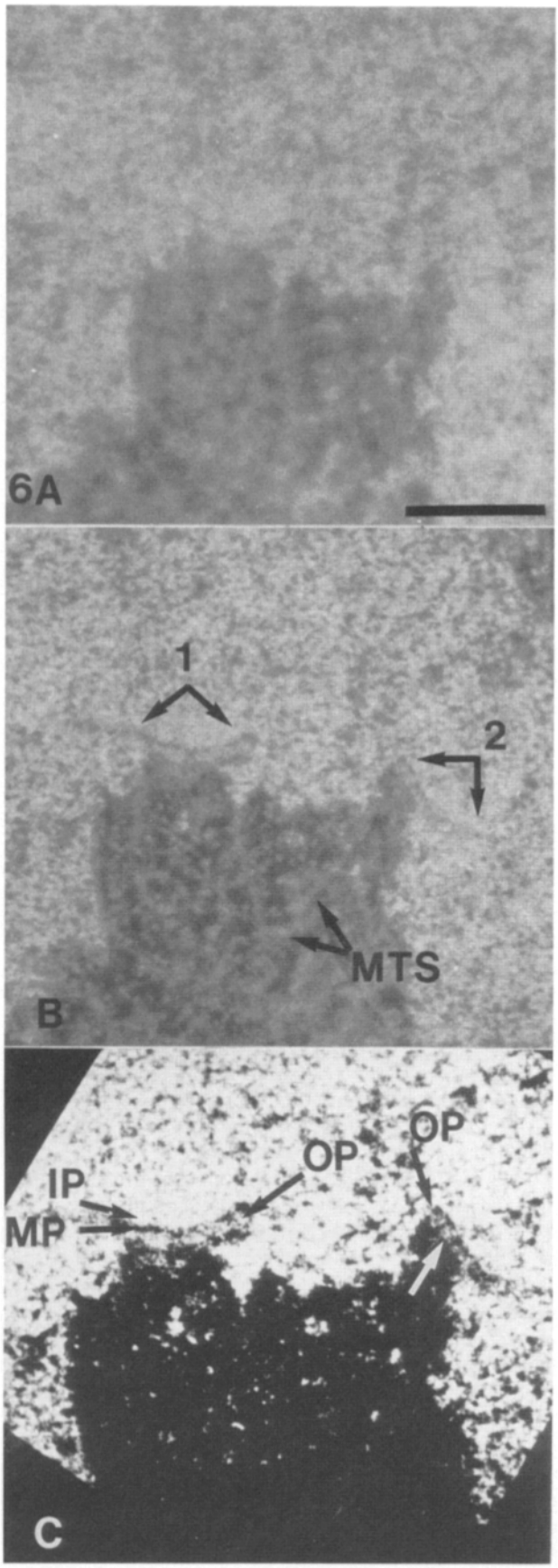

Figure 6. The reference (*A*), phosphorus-enhanced (*B*), and net phosphorus (*C*) images of a region of a telophase cell in which two kinetochore regions (*1* and *2*) no longer associated with the mitotic spindle are being enveloped by decondensing chromatin. Short remnants of the spindle microtubules (*MTS*) are seen in the adjacent cytoplasm. In both kinetochores, the phosphorus distribution is identical to that found in fully functional (Fig. 3) and colcemid treated (Fig. 1) kinetochores. *IP*, inner plate; *MP*, middle plate; *OP*, outer plate. Bar, 0.6 μm.

traverses this region (Fig. 4 *C*, *black arrow*). This phosphorus-rich region is generally 30 nm in diameter and in favorable sections appears continuous with both the inner and outer plate. This arrangement suggests that the band represents the passage of the 30-nm kinetochore fiber between the inner and outer plates. The region containing the fibrous corona is also devoid of a strong phosphorus signal (Fig. 3 *C* and Fig. 4, *A–C*) and generally excludes even the somewhat dense granular phosphorus pattern that is characteristic of the adjacent cytoplasm.

The distribution of phosphorus in each of the regions described in the previous section is not altered by the associations of spindle microtubules with the kinetochore (Fig. 5). However, the substructure of the kinetochore is partially obscured because the microtubules also produce a phosphorus signal. Most of the signal due to the microtubules terminates at the outer plate. Occasionally, however, a microtubule appears to insert between adjacent kinetochore fiber profiles and extends directly into the lower plate (Fig. 5, also see Fig. 7 *A*). Whereas it is not possible to identify the kinetochore in interphase nuclei, it is possible to identify these structures in telophase cells just before the reassembly of the nuclear envelope and after the disappearance of microtubule profiles from the surface of the kinetochore (Fig. 6, *A*, *B*, and *C*). At this stage the three layers of the kinetochore can still be seen in favorable sections although the outer layer is beginning to be enveloped by a layer of chromatin from outside the kinetochore region. Electron spectroscopic imaging indicates that the distribution of phosphorus remains the same in these now functionally inactive kinetochores. Therefore, the state of activity of the kinetochore does not appear to alter the phosphorus distribution. Short microtubules representing residual elements of the mitotic spindle are seen in the cytoplasm adjacent to the reforming nucleus (Fig. 6). Interestingly, these profiles do not contain a detectable level of phosphorus as they do in microtubules of the active spindle.

The Relationship of the Kinetochore to Spindle Microtubules

The relationship between the structure of the kinetochore and spindle microtubules can be determined by the evaluation of images obtained by conventional transmission electron microscopy in concert with information obtained by ESI. Care must be taken in interpretation of conventional micrographs since there is a possibility of superimposition in 60–90-nm-thick sections. In addition, microtubules might sharply pass out of the plane of the section rather than terminate at the point apparent in the micrograph. With these factors in mind, microtubules appear to terminate in three different regions in cross sections viewed by conventional microscopy. The majority of the microtubules terminate at the level of the outer plate. However, a small population extend through the outer plate, traverse the middle plate, and

terminate in the inner plate. In addition, a few microtubules confined to the periphery of the kinetochore pass through the kinetochore region and insert directly into the underlying chromatin (Fig. 7 *A*). This relationship can also be seen in longitudinal sections through the plate (Fig. 7 *B*) and is compatible with the images obtained by ESI where section thickness is reduced and resolution enhanced.

The kinetochore of the Indian muntjac are extremely large and at metaphase there is stress placed on the plate by the spindle microtubules. Therefore, the kinetochore does not always remain flat but may have an undulating surface. Thus the outer plate can exist at two different levels within a region encompassed by a single conventional thin section (Fig. 7 *C*). Further whole mount preparations indicate that the kinetochore fibers do not form perfectly regular rows but follow a curved course so that they would be expected to pass in and out of the plane of a section cut along the fiber (4). Since the section thickness is 60–90 nm (silver to gold range), the features described above suggest that it should be possible to view several longitudinal profiles of the kinetochore fiber (30 nm) and microtubule profiles (25 nm) in the same section. This expectation is satisfied by the images presented in Fig. 7, *D*, *E*, and *F*. In Fig. 7 *E*, portions of two passages of the kinetochore fiber can be viewed in addition to the middle and lower plates. In each case, the fiber does not pass across the whole profile of the kinetochore but rather passes in and out of the plane of the section. In regions that coincide with the passage of the fiber out of the plane of the section microtubule profiles come into view. This arrangement suggests that the microtubules are positioned between the rows of chromatin fibers, a relationship also reinforced by the images illustrated in Fig. 5, *E* and *F*. It should be noted that the apparent center-to-center spacing (55–60 nm) of cross-sectional profiles of microtubules at the surface of the outer plate are large enough to accommodate the passage of a kinetochore fiber between the profiles (Fig. 7 *B*).

Discussion

Electron spectroscopic imaging illustrates that the kinetochore is both differentiated in terms of its structure and phosphorus distribution. Most of the phosphorus is associated with profiles of a 30-nm kinetochore fiber. The high phosphorus signal associated with this fiber, together with evidence that it is susceptible to nucleases, support the notion that this fiber contains DNA and probably represents a chromatin organization unique to the kinetochore domain. In addition, the phosphorus distribution signal indicates that the majority of the fiber is confined to the kinetochore inner and outer plates. The middle plate is largely devoid of phosphorus and appears to contain only short portions of the phosphorus-containing fiber. The lack of detectable structure within the middle plate suggests that this region may be better considered a space rather than a plate. Thus, the kinetochore can be viewed as a structure with an inner space, a feature that may have functional implications. For example, several lines of evidence suggest that kinetochores move along spindle microtubules by depolymerization at the kinetochore (15, 16). If most of the kinetochore microtubules end at the outer plate then depolymerization probably occurs at the interface between the outer and middle plates. The presence of space in this region may act as reservoir for tubulin subunits and for factors that regulate microtubule structure.

The presence of autoantibodies to a variety of kinetochore antigens has facilitated the identification of a number of unique kinetochore proteins (17). Although the function and precise localization of these proteins in the kinetochore is not known, some may play a structural role in the integration of neighboring kinetochore fibers and the formation of the plates. Control of the assembly and disassembly of the plates during the cell cycle, for example, may be related to phosphorylation levels of these proteins. The appearance of a phosphorus signal in regions of the inner and outer plate between the kinetochore fibers may reflect the distribution of such proteins. Although several lines of evidence suggest that the kinetochore fiber contains DNA, we cannot at present rule out the possibility that phosphorylated proteins are also directly associated with the kinetochore fiber and contribute to the signal. We have not been able to detect a phosphorylation–dephosphorylation cycle for kinetochore phosphoproteins within the period studied.

The fibrous corona is a component of the kinetochore that is particularly evident in kinetochores that lack microtubule association. Our study indicates that this region is not highly phosphorylated. It is composed of a series of fine fibers that are arranged into rows along the surface of the kinetochore outer plate (1, 2). Although our study does not indicate the precise relationship between the kinetochore fiber and the corona, it seems reasonable to assume that they interact with the kinetochore fibers and are probably arranged in rows along the surface of the outer plate. Such an arrangement would give the surface of the kinetochore the appearance of a hair brush. If the corona plays a role in the initial capture of spindle microtubules, the hair brush arrangement may function to facilitate this process and guide microtubules down to attachment sites along the rows of the kinetochore fiber. The site at which microtubules interact with the laterally placed kinetochore fiber may be specified by sequences similar, at least in function if not in sequence composition, to the yeast CEN sequences. The distribution of these sites along the fiber could specify the periodic association of the microtubules with the outer plate. A small percentage of microtubules extend through the outerplate and into the lower plate. Our ESI studies suggest that the lower plate also contains kinetochore fibers that are arranged in a precise manner. Therefore, the organization of the inner plate may mimic that found in the outer plate in that the arrangement facilitates the interaction of microtubules with specific DNA sequences. The differential distribution of these sequences, however, may reflect functional differences and indicate that these microtubules represent separate functional classes or states.

In conclusion, electron spectroscopic imaging of the kinetochore supports the type of model of kinetochore structure proposed by Rattner (4) and Ris and Witt (3). We can now specify with some certainty the distribution of the kinetochore fiber in each of the kinetochore layers and the relationship of the fibrous corona and spindle microtubules to the kinetochore. The complex architecture of the kinetochore can be correlated with the highly complex role this chromosomal domain plays during cell division. Our study also illustrates the ability of electron spectroscopic imaging techniques to provide both high resolution images and elemental

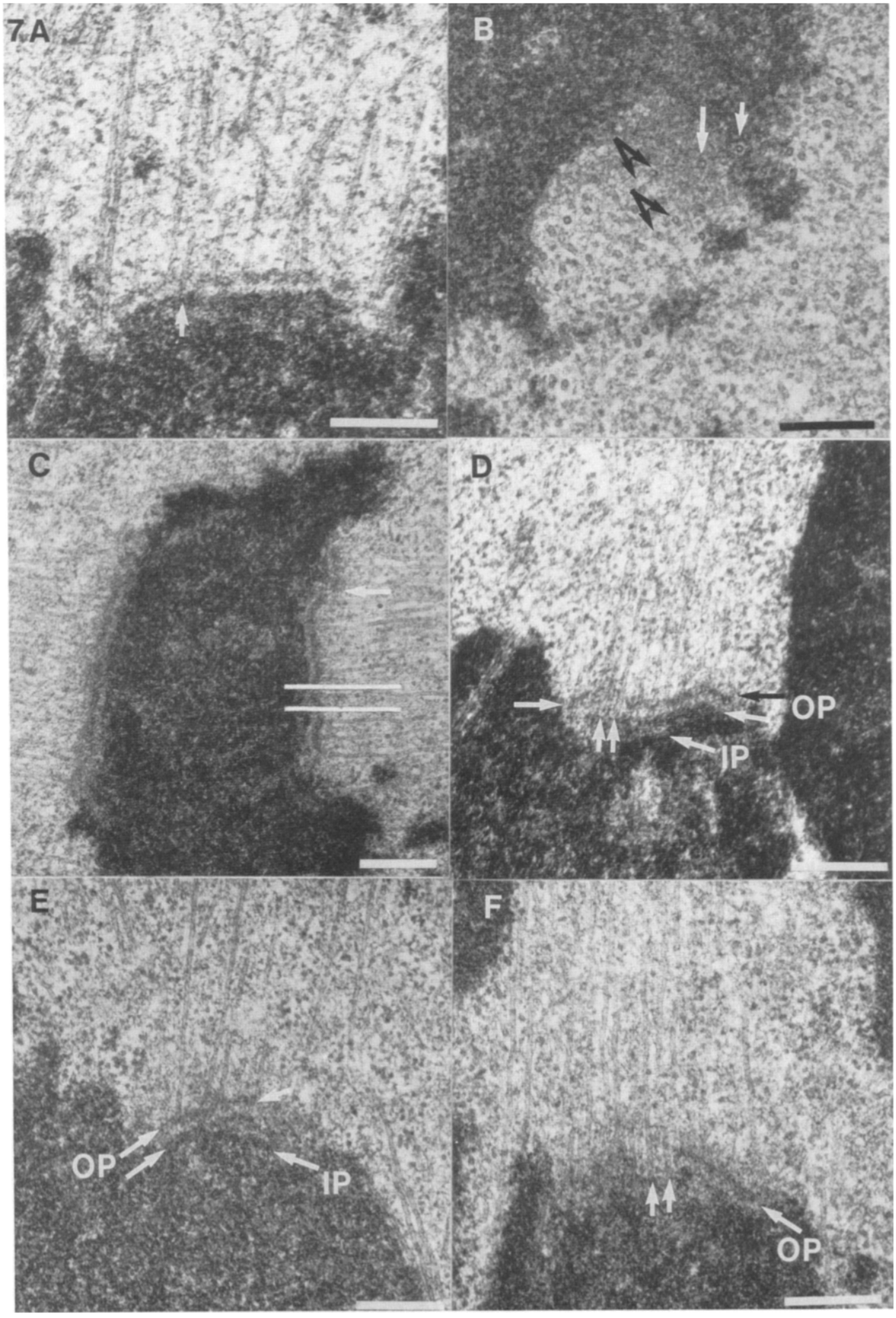
7A
B
C
D
OP
IP
E
OP
IP
F
OP

information. This information facilitates the determination of structural and functional correlates. We are currently investigating the precise distribution of kinetochore-specific proteins using affinity-purified antibodies that have been labeled in a manner that can be detected by ESI.

The authors would like to thank Teresa Wang for her excellent technical assistance.

This work was supported by a grant from the National Cancer Institute of Canada (to J. B. Rattner) and from the Medical Research Council of Canada (to D. P. Bazett-Jones).

Received for publication 24 October 1988.

References

1. Bazett-Jones, D. P., and F. P. Ottensmeyer. 1981. Phosphorus distribution in the nucleosome. *Science (Wash. DC).* 211:169–170.
2. Bazett-Jones, D. P., L. Locklear, and J. B. Rattner. 1988. Electron spectroscopic imaging of DNA. *J. Ultrastruct. Mol. Struc. Res.* 99:48–58.
3. Brinkley, B. R., and E. Stabblefield. 1970. Ultrastructure and interaction of the kinetochore and centriole in mitosis and meiosis. *In* Advances in Cell Biology. Vol. 1 D. M. Prescott, L. Goldstein, and E. McConkey, editors. Appleton-Century-Crofts, New York. 119–185.
4. Brinkley, B. R., M. M. Valdivia, A. Tousson, and S. L. Brenner. 1984. Compound kinetochore of the Indian muntjac. *Chromosoma (Berl.).* 91:1–11.
5. Earnshaw, W. C., and N. Rothfield. 1985. Identification of a family of human centromere proteins using sera from patients with scleroderma. *Chromosoma (Berl.).* 91:313–319.
6. Edgerton, R. F. 1975. Ineleastic features of 80 KeV electrons in amorphous carbon. *Philos. Mag.* 31:199–215.
7. Gorbsky, G. J., P. L. Sammak, and G. G. Borisy. 1987. Chromosomes move poleward in anaphase along stationary microtubules that coordinately disassemble from their kinetochore ends. *J. Cell Biol.* 104:9–18.
8. Jokelainen, P. T. 1967. The ultrastructure and spatial organization of the metaphase kinetochore in mitotic rat cells. *J. Ultrastruct. Res.* 16:19–44.
9. Mitchison, T. L., E. Evans, E. Schultze, and M. Kirschner. 1986. Sites of microtubule assembly and disassembly in the mitotic spindle. *Cell.* 45:515–527.
10. Palmer, D. K., and R. L. Margolis. 1985. Kinetochore components recognized by human autoantibodies are present on mononucleosomes. *Mol. Cell. Biol.* 5:173–186.
11. Rattner, J. B. 1986. Organization within the mammalian kinetochore. *Chromosoma (Berl.).* 93:515–520.
12. Rattner, J. B. 1987. The organization of the mammalian kinetochore: a scanning electron microscope study. *Chromosoma (Berl.).* 95:175–181.
13. Rattner, J. B., and C. C. Lin. 1985. Radial loops and helical coils coexist in metaphase chromosomes. *Cell.* 42:291–296.
14. Rattner, J. B., and C. C. Lin. 1987. The higher order structure of the centromere. *Genome.* 29:588–594.
15. Ris, H., and P. L. Witt. 1981. Structure of the mammalian kinetochore. *Chromosoma (Berl.).* 82:153–167.
16. Roos, U. P. 1973. Light and electron microscopy of rat kangaroo cells in mitosis II. Kinetochore structure and function. *Chromosoma (Berl.).* 41:195–220.
17. Valdivia, M. W., and B. R. Brinkley. 1985. Fractionation and initial characterization of the kinetochore from mammalian metaphase chromosomes. *J. Cell Biol.* 101:1124–1134.

Figure 7. Conventional electron micrographs of the several kinetochores of the Indian muntjac. In longitudinal section (*A*), microtubules can be seen inserting into the outer plate, inner plate (*arrow*), and the chromatin adjacent to the kinetochore. This distribution can also be detected in cross sections through the plate (*B*). Profiles in the inner plate and lateral to the plate are indicated by the white arrows. In the outer plate, the microtubule profiles have a center-to-center spacing of 550–600 nm (*black arrows*). The surface of the kinetochore frequently has an undulating appearance (*C, white brackets*). Therefore, in sections that are cut 90° from that shown in *C* and that also contain longitudinal profiles of the kinetochore fiber, it is possible to visualize several of the 30-nm fibers (*parallel arrows*) at the same time (*D, E,* and *F*). Analysis of the relationship of the microtubule profiles (*arrows perpendicular to the plate*) to the fiber profiles suggest that microtubules insert between adjacent rows of the kinetochore fiber (*D, E,* and *F*). *IP,* inner plate; *MP,* middle plate; *OP,* outer plate. Bar, 0.5 μm.